Acta Crystallographica Section D
Biological Crystallography
ISSN 0907-4449

Fine-tuning of prototype chicken galectins: structure of CG-2 and structure–activity correlations

Federico M. Ruiz,[a]‡ Israel S. Fernández,[a]‡ Lara López-Merino,[b,c]‡ Laura Lagartera,[c] Herbert Kaltner,[d] Margarita Menéndez,[b,c] Sabine André,[d] Dolores Solís,[b,c]* Hans-Joachim Gabius[d] and Antonio Romero[a]*

[a]Departamento de Biología Físico-Química, Centro de Investigaciones Biológicas – CSIC, Ramiro de Maeztu 9, 28040 Madrid, Spain, [b]Departamento de Química-Física Biológica, Instituto de Química Física Rocasolano – CSIC, Serrano 119, 28006 Madrid, Spain, [c]Centro de Investigación Biomédica en Red de Enfermedades Respiratorias (CIBERES), 07110 Bunyola, Mallorca, Illes Balears, Spain, and [d]Institut für Physiologische Chemie, Tierärztliche Fakultät, Ludwig-Maximilians-Universität, Veterinärstrasse 13, 80539 München, Germany

‡ These authors contributed equally to this work.

Correspondence e-mail: d.solis@iqfr.csic.es, romero@cib.csic.es

Received 7 March 2013
Accepted 30 April 2013

PDB Reference: chicken galectin 2, 2ymz

The comparatively small number of members of the family of adhesion/growth-regulatory galectins in chicken predestines this system as an attractive model to study the divergence of these lectins after gene duplication. Expression profiling of the three homodimeric (prototype) chicken galectins (CG-1A, CG-1B and CG-2) has raised evidence of distinct functionalities, explaining the interest in a detailed crystallographic analysis of CG-2. As revealed here, marked differences are found in the ligand-binding site and in the contact pattern within the homodimer interface, underlying a characteristic orientation of the two subunits. Notably, a distinctive trimer of dimers that is unique in all galectin crystal structures reported to date forms the core unit of the crystallographic assembly. Combination with spectroscopic and thermodynamic measurements, and comparisons with CG-1A and CG-1B, identify differential changes in the circular-dichroism spectra in the presence of lactose, reflecting the far-reaching impact of the ligand on hydrodynamic behaviour, and inter-galectin differences in both the entropy and the enthalpy of binding. This structural information is a salient step to complete the analysis of the full set of galectins from this model organism.

1. Introduction

The central role of lectins in initiating the translation of sugar-encoded information into physiological responses explains the interest in defining their structures (Gabius, 2009; Gabius *et al.*, 2011). The members of the family of adhesion/growth-regulatory galectins share a distinct sequence signature, a β-sandwich fold with a central Trp residue in the binding site and affinity for lactose (Barondes *et al.*, 1994; Kasai & Hirabayashi, 1996; Gabius, 1997; Villalobo *et al.*, 2006; Klyosov *et al.*, 2008; Schwartz-Albiez, 2009; Smetana *et al.*, 2013). They are divided into three groups based on the mode of presentation of their carbohydrate-recognition domain(s) (CRD). Monomeric and homodimeric proteins belong to the prototype category, while the covalent association of the CRD with two other modules (collagen-like repeats and a peptide terminus with sites for Ser phosphorylation) leads to the chimera-type design, and the chain-like display of up to four different CRDs covalently connected by linker peptide(s) is characteristic of the tandem-repeat-type proteins (Kasai & Hirabayashi, 1996; Cooper, 2002; Tasumi & Vasta, 2007). Respective genes for these three groups are invariably found in vertebrates (Cooper, 2002; Houzelstein *et al.*, 2004). Gene duplications and the ensuing sequence divergence have given rise to different levels of complexity in the overall organization of the species-specific galectin profile. Obviously, an organism with a rather low extent of diversification is best

suited for performing a comprehensive comparative analysis of the network comprising the three described classes. Based on this criterion, the chicken genome is an attractive model candidate. It harbours a total of only five genes for functional galectins (Cooper, 2002; Houzelstein *et al.*, 2004; Kaltner & Gabius, 2012).

We have previously reported the crystal structures of two prototype proteins, *i.e.* the paralogue pair CG-1A and CG-1B (Varela *et al.*, 1999; López-Lucendo *et al.*, 2009). The third prototype CG, *i.e.* CG-2, is assumed to have arisen from a duplication event prior to the emergence of the CG-1A and CG-1B genes (the orthologues of human galectin-1; hGal-1) and, as indicated by its designation, CG-2 is suggested to be orthologous to human galectin-2 (hGal-2; for sequence comparisons, see Fig. 1; Hirabayashi *et al.*, 1987; Sakakura *et al.*, 1990; Houzelstein *et al.*, 2004; Kaltner *et al.*, 2008).

CG-2 was first purified from adult chicken intestine and was subsequently detected to be strongly expressed in embryonic kidney (Beyer *et al.*, 1980; Beyer & Barondes, 1982; Stierstorfer *et al.*, 2000). Its immunohistochemical expression profile, with a presence in the epithelial lining of villi and intestinal glands as well as the collecting ducts in adult kidney, is mostly different from those of the other two prototype CGs (Kaltner *et al.*, 2008; Kaltner & Gabius, 2012). Its presence in the digestive tract is shared by mammalian galectin-2, as revealed by analysis of human, mouse, pig and rat tissues (Oka *et al.*, 1999; Saal *et al.*, 2005; Lohr *et al.*, 2007; Thomsen *et al.*, 2009; Nio-Kobayashi *et al.*, 2009), and delineation of the profile of caspase involvement in the induction of apoptosis of activated T cells revealed functional divergence among human prototype galectins (Sturm *et al.*, 2004). In this respect CG-1A was very active, while CG-2 showed selective B-cell-binding capacity among avian immune cells (Schneller *et al.*, 1995; Kaltner *et al.*, 2008). On examination of the lectin sites of CG-2 and CG-1A in solution, chemical mapping detected initial evidence for quantitative differences in the capacity of CG-2 to bind β-lactoside derivatives relative to CG-1A (Solís *et al.*, 1996).

Here, we report the structure of CG-2. Owing to the availability of corresponding data for hGal-1 and hGal-2 (Lobsanov *et al.*, 1993; López-Lucendo, Solís *et al.*, 2004), the proposed relationships between the avian and mammalian proteins could then likewise be tested. On the grounds of models of the binding of disaccharides to pentasaccharides to CG-1A, CG-1B, hGal-1 and hGal-2, along with glycan-array data for the human lectins (Siebert *et al.*, 2003; André *et al.*, 2005; Wu *et al.*, 2007; Stowell *et al.*, 2008), making assumptions about how affinity and specificity are altered during the course of sequence divergence appears to be possible. Flanking the crystallographic work, we carried out analytical experiments in solution with the three prototype CGs. Since circular-dichroism (CD) spectroscopy has proven its value as a sensor for fine structural alterations upon ligand binding in the case of human galectins (Nesmelova *et al.*, 2010; Solís *et al.*, 2010), we extended our comparison accordingly, adding determination of thermal stability in the absence and presence of lactose. The thermodynamics of lactose binding was also measured in order to answer the question of enthalpic/entropic contributions to binding in each case.

2. Materials and methods

2.1. Protein expression and purification

The complete cDNA for CG-2 was cloned from total RNA of embryonic kidney (developmental day 15) and was inserted into the vector pQE60 (Qiagen, Hilden, Germany). *Escherichia coli* strain M15 (pREP4) was used for recombinant protein production of the product, which is identical to the physiological form, as described by Kaltner *et al.* (2008). As provided therein, the sequence of the full-length cDNA including the first exon (two amino acids; methionine and alanine) is identical to the respective GenBank entries XM_00123499.2 (mRNA) and XM_00123499.2 (protein) and is also completely in line with the genomic sequence (Gene ID 425107). Following purification by affinity chromatography on lactosylated Sepharose 4B as a crucial step, controls for purity and activity assays were performed as described elsewhere (Gabius *et al.*, 1984; Kaltner *et al.*, 2008; Amano *et al.*, 2012; André *et al.*, 2012). Production and quality controls of CG-1A,

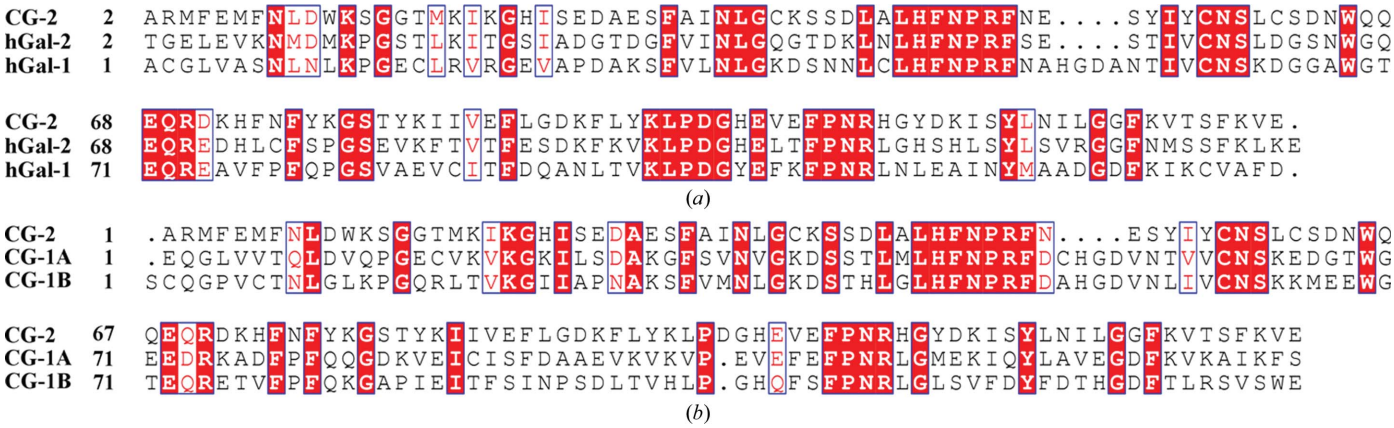

Figure 1
Sequence alignment of CG-2 with (*a*) those of human galectin-1 and galectin-2 (hGal-1 and hGal-2) and (*b*) those of the other two prototype CGs (CG-1A and CG-1B). Strictly conserved residues (red background) and homologous residues (>70% conservation; boxed red letters) are shown.

Table 1
Data-collection and refinement statistics.

Values in parentheses are for the outermost resolution shell.

Data collection	
Space group	$P2_12_12_1$
Unit-cell parameters (Å)	a = 65.85, b = 90.70, c = 151.66
Resolution (Å)	43.6–1.75 (1.84–1.75)
R_{merge}†	0.065 (0.479)
$\langle I/\sigma(I)\rangle$	5.7 (1.6)
Completeness (%)	98.0 (88.6)
Multiplicity	6.5 (3.8)
Reflections measured	587745 (44993)
Unique reflections	90417 (11740)
Wilson B factor (Å^2)	25.05
Mosaicity (°)	0.2
Refinement	
Resolution (Å)	43.6–1.75
No. of reflections	85820 (4511)
R_{work}‡/R_{free} (%)	18.9/22.7
No. of atoms	
Protein	6354
Ligand/ion	46
Water	507
B factors (Å^2)	
Protein	30.05
Ligand/ion	53.2
Water	40.5
R.m.s. deviations	
Bond lengths (Å)	0.019
Bond angles (°)	2.171

† $R_{merge} = \sum_{hkl}\sum_i |I_i(hkl) - \langle I(hkl)\rangle| / \sum_{hkl}\sum_i I_i(hkl)$, where $I_i(hkl)$ is the measurement of the intensity for each reflection and $\langle I(hkl)\rangle$ is the mean intensity of that reflection. ‡ $R_{work} = \sum_{hkl} ||F_{obs}| - |F_{calc}|| / \sum_{hkl} |F_{obs}|$, where F_{obs} and F_{calc} are the observed and calculated structure-factor amplitudes, respectively. R_{free} is calculated as for R_{work} but for a subset of randomly chosen reflections (5%) which were not used in structure refinement.

CG-1B and its C7S mutant were also carried out as described previously (Wu *et al.*, 2007; López-Lucendo *et al.*, 2009) and mass-spectrometric fingerprint analyses of native and thermally denatured CG-1B and its mutant were performed after alkylation with 80 m*M* iodoacetamide in the presence of 9 *M* urea for 1 h at 293 K in the dark without prior reduction (López-Lucendo *et al.*, 2009).

2.2. Crystallization, data collection and processing

For crystallization experiments, the CG-2-containing solution was dialyzed against a buffer consisting of 5 m*M* potassium/sodium phosphate, 150 m*M* NaCl, 10 m*M* lactose, 4 m*M* β-mercaptoethanol pH 7.2 and was concentrated to 5 mg ml^{-1} using a Centricon-10 ultrafiltration unit (Millipore). Initial crystallization trials were performed at room temperature using the sitting-drop vapour-diffusion method with commercial screening solutions including Crystal Screen and Crystal Screen 2 (Hampton Research), JBScreen Basic 1–4 (Jena Bioscience) and Wizard III (Emerald BioSciences). Sitting drops were prepared by mixing 0.2 µl protein solution and 0.2 µl reservoir solution in 96-well MRC plates (Swissci) using a Synquad nanodispenser robot (Cartesian). Based on this initial screening, crystals were obtained using condition Nos. 32 and 47 of Crystal Screen and condition No. 24 of Wizard III, all of which contained 2.0 *M* ammonium sulfate. These conditions were further optimized and single crystals reaching maximum dimensions of 0.1 × 0.1 × 0.1 mm were obtained over the course of a week. The final optimized condition was 2 *M* ammonium sulfate, 0.1 *M* sodium acetate pH 4.8, 1%(*v*/*v*) β-mercaptoethanol. For data collection, crystals were rapidly transferred into a cryosolution consisting of reservoir solution supplemented with 20%(*v*/*v*) glycerol and flash-cooled in liquid nitrogen.

X-ray diffraction data were collected to 1.75 Å resolution on the ID14-2 beamline at the ESRF, Grenoble, France using a single cooled crystal (100 K). A total of 180° of data were collected with a 1° oscillation angle and an exposure time of 1 s. The diffraction images were processed with *MOSFLM* (Leslie, 2006). Data scaling, merging and reduction were carried out with programs from the *CCP*4 suite (Winn *et al.*, 2011). The CG-2 crystals belonged to space group $P2_12_12_1$, with unit-cell parameters a = 65.85, b = 90.70, c = 151.66 Å. $I/\sigma(I)$ fell below 2.0 at 1.79 Å resolution. However, to determine the highest resolution cutoff for our data we used the correlation coefficient $CC_{1/2}$ (Karplus & Diederichs, 2012). A value of 72.6% for the highest resolution shell supported our high-resolution limit of 1.75 Å. Data-collection statistics are listed in Table 1.

2.3. Structure determination and refinement

An estimate of the solvent content of the CG-2 crystals (Matthews, 1968) suggested the presence of between four (V_M = 3.79 Å^3 Da^{-1}) and six (V_M = 2.52 Å^3 Da^{-1}) molecules in the asymmetric unit. Self-rotation analysis showed peaks corresponding to threefold (κ = 120°; parallel to the y axis) and twofold (κ = 180°; in the xz plane) axes, indicating the probable presence of six CG-2 molecules in the asymmetric unit.

The structure of CG-2 was determined by molecular replacement using *MOLREP* (Vagin & Teplyakov, 2010) and *Phaser* (McCoy *et al.*, 2007) from the *CCP*4 suite (Winn *et al.*, 2011). The structure of CG-1A (40% sequence identity; PDB entry 1qmj; Varela *et al.*, 1999) was used as the search probe with data to 3.5 Å resolution. The initial rotational and translational searches using *MOLREP* only identified four monomers of the hexamer in the asymmetric unit. The best solution had an R factor and a *MOLREP* score of 0.615 and 0.188, respectively. This partial solution was then refined using *REFMAC* (Murshudov *et al.*, 2011). Subsequently, searches for the two remaining units were performed using *Phaser* (McCoy *et al.*, 2007), keeping the already detected tetramer fixed and using the model of one of the CG-2 units as the probe in a new query. A solution comprising six monomers (TFZ = 16.5, LLG = 479) was obtained and refined by several rounds of simulated annealing followed by further cycles of B-factor improvement with noncrystallographic symmetry restraints. The final R_{work} and R_{free} values were 18.9 and 22.7%, respectively. Manual model-building/refinement cycles were performed using *Coot* (Emsley *et al.*, 2010) and *REFMAC* (Murshudov *et al.*, 2011). Water molecules were gradually added during further conjugate-gradient refinement using *Coot* (Emsley *et al.*, 2010). The stereochemistry of the final model was validated using *MolProbity* (Chen *et al.*, 2010); no

residues were within prohibited regions of the Ramachandran plot. Protein–protein interactions were analysed using the *PISA* web server (Krissinel & Henrick, 2007). The refinement statistics are summarized in Table 1.

2.4. Circular dichroism

CD spectra were acquired with a J-810 spectropolarimeter (Jasco) equipped with a Peltier temperature-control system using a bandwidth of 1 nm and a response time of 4 s. Far-UV spectra were recorded in 0.1 cm path-length quartz cells at a protein concentration of 0.2 mg ml^{-1} in 5 m*M* sodium phosphate buffer pH 7.2 containing 0.2 *M* NaCl and 4 m*M* β-mercaptoethanol (PBS$_\beta$), while near-UV spectra were recorded at protein concentration 1.0 mg ml^{-1} in 1 cm path-length cells. The buffer contribution was subtracted from the raw protein data. Thermal denaturation experiments were carried out by increasing the temperature from 303 to 363 K at a scanning rate of 0.66 K min^{-1}. Spectra were recorded every 10 K and variations in ellipticity at a selected wavelength were monitored every 0.2 K. Thermal denaturation profiles were described in terms of one or two sigmoidal functions

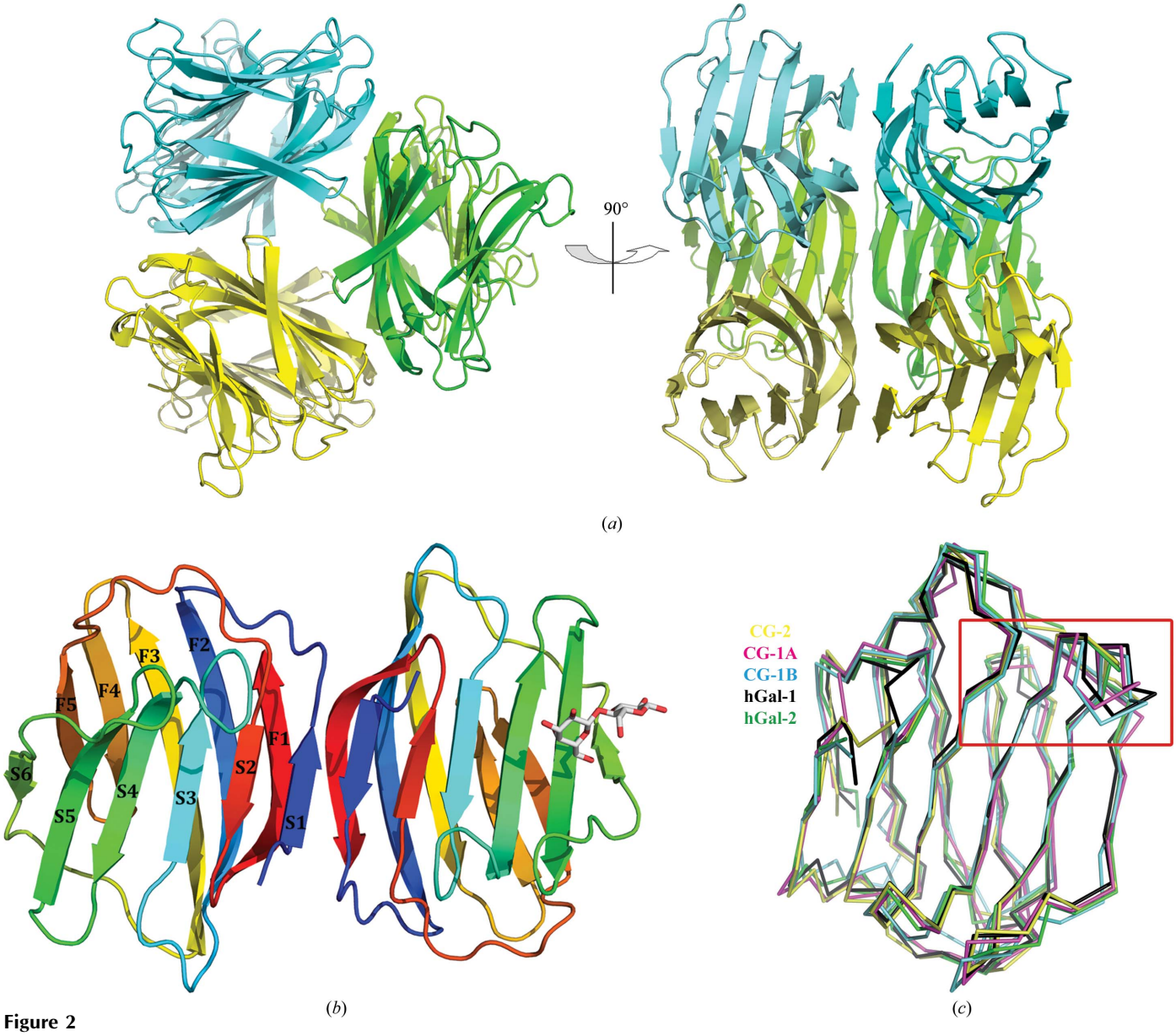

Figure 2
Overall structure of CG-2. (*a*) Two different views of the asymmetric unit containing a total of six CG-2 units arranged as three dimers. The two subunits of each dimer (coloured yellow, cyan and green) are related by a noncrystallographic twofold axis. (*b*) The CG-2 monomer adopts the typical β-sandwich fold formed by two antiparallel β-sheets of six (S1–S6) and five (F1–F5) β-strands. The lactose molecule in the binding site of the right subunit is shown in stick mode. (*c*) Superimposition of the C$^\alpha$ atoms of members of the prototype group, *i.e.* CG-2 (yellow), CG-1A (PDB entry 1qmj; Varela *et al.*, 1999; magenta), CG-1B (PDB entry 3dui; López-Lucendo *et al.*, 2009; cyan), hGal-1 (PDB entry 1gzw; López-Lucendo, Solís *et al.*, 2004; black) and hGal-2 (PDB entry 1hlc; Lobsanov *et al.*, 1993; green) (for sequences, see Fig. 1). The region displaying the largest deviation (the S4–S5 loop) is boxed. Figures were prepared using *PyMOL* (DeLano, 2002).

(Campanero-Rhodes *et al.*, 2006), depending on the number of transitions observed, using the equation

$$\Theta(T) = \frac{\Theta_N + \sum_{i=1}^{n} \Delta\Theta_i \{\exp[-HD_i(T_{1/2i} - T)/R \cdot T_{1/2i} \cdot T]\}}{\{1 + \exp[-HD_i(T_{1/2i} - T)/R \cdot T_{1/2i} \cdot T]\}}, \quad (1)$$

where $\Theta(T)$ is the ellipticity at absolute temperature T, Θ_N is the ellipticity of the native state, n is the number of transitions, $\Delta\Theta_i$ is the variation in ellipticity associated with transition i, $T_{1/2i}$ and HD_i are the half-transition temperature and the parameter accounting for the cooperativity of the respective transition, respectively, and R is the gas constant.

2.5. Isothermal titration calorimetry (ITC)

ITC measurements were carried out at 298 K in PBS_β buffer using a VP-ITC microcalorimeter (MicroCal) as described by Martín-Santamaría *et al.* (2011). Alternatively, 5 m*M* HEPES pH 7.2 containing 0.2 *M* NaCl and 4 m*M* β-mercaptoethanol ($HEPES_\beta$), a buffer with an ionization enthalpy that is quite different from that of phosphate, was used to evaluate the possible contribution of protein–buffer proton exchange resulting from variations in the pK_a values of protein groups upon lactose binding. Before measurements, protein samples were exhaustively dialyzed against the corresponding buffer and lactose solutions for titrating galectin samples were prepared using the last dialysis buffer. The heat developed on lactose dilution was determined in separate runs and was subtracted from the apparent heat of reaction. The thermodynamic parameters were calculated by analysing the binding isotherms using the MicroCal *Origin* software. The monomer concentration of the lectins was used as input in the fitting procedures.

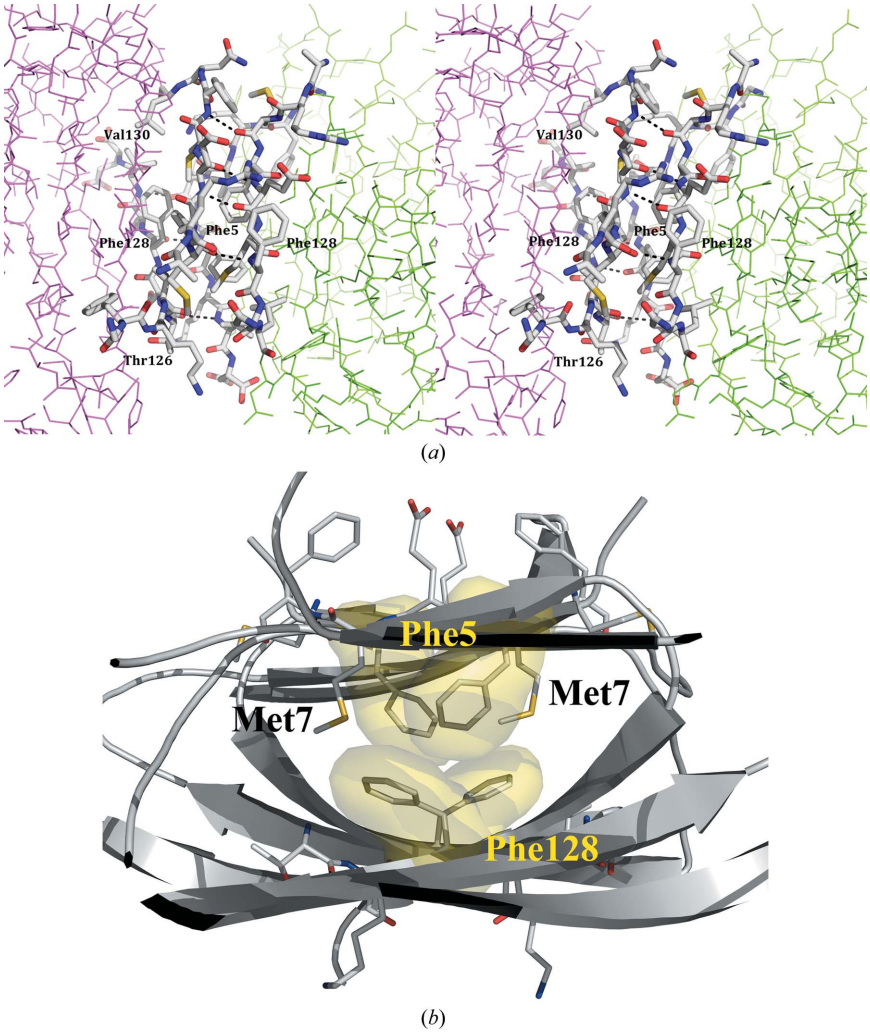

Figure 3
Overview of the canonical interface of the CG-2 dimer. (*a*) The S1 and F1 β-strands from the N- and C-termini are in the contact region, facilitating both polar and hydrophobic interactions. (*b*) The special distribution of nonpolar side chains in both the S1 and F1 strands establishes a hydrophobic surface. Most notable is the involvement of the side chains of Phe5 and Phe128 within the core of the hydrophobic pocket (yellow). In addition, CG-2 extends the hydrophobic core through additional methionine side chains at positions 4 and 7.

3. Results and discussion

3.1. Overall description of the structure

The crystal structure of CG-2 was determined at 1.75 Å resolution by molecular replacement using the previously published structure of CG-1A (PDB entry 1qmj; Varela *et al.*, 1999) as a search probe. Statistics of data processing and refinement parameters of the structure are presented in Table 1. The final model comprises a total of six monomers of 130 residues each, two lactose molecules and 507 water molecules. The asymmetric unit in the crystal contains three CG-2 dimers, in which the two subunits of each dimer are related by a noncrystallographic twofold axis. Thus, the crystal organization can be viewed as a noncrystallographic trimer of dimers (Fig. 2*a*). Initial sedimentation-equilibrium analyses at loading concentrations between 0.1 and 1 mg ml^{-1} had shown CG-2 to be completely dimeric (Kaltner *et al.*, 2008), and gel filtration had also so far not provided evidence for oligomerization (Beyer *et al.*, 1980; Kaltner *et al.*, 2008). However, the concentration could have a marked impact. To test this assumption, further sedimentation-velocity analyses were carried out at a higher protein concentration (4 mg ml^{-1}). They revealed the presence of a predominant peak (70% of the total protein) with a sedimentation coefficient of 2.3 S ($s_{20,w}$) corresponding to the CG-2 dimer, together with species with

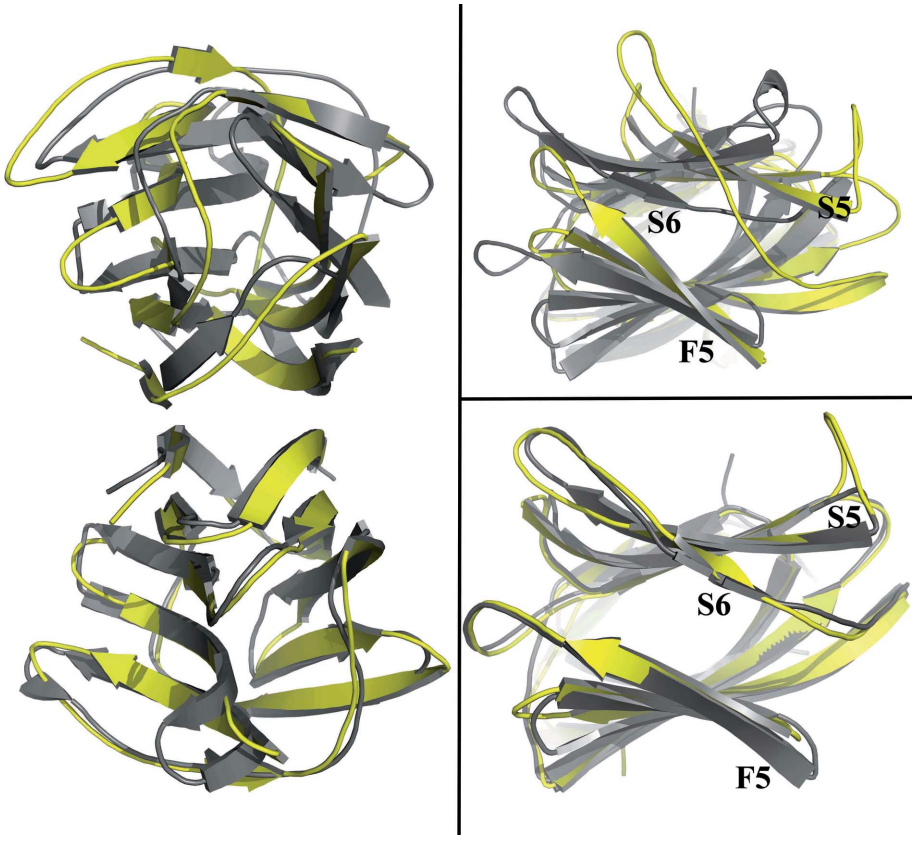

Figure 4
Comparison of the dimer arrangement (left) in CG-2 (grey) and hGal-1 (yellow). The superposition is based on one subunit of CG-2 and yielded an r.m.s.d. deviation of 0.4 Å for 130 residues. On the right a separated view of the superposition from the bottom (lower panel) and from the top (upper panel) is shown. As can be seen, a large rotation must be applied to bring the second subunit of the CG-2 dimer into the equivalent position in hGal-1.

$s_{20,w}$ values of 3.4 and 5.7 S accounting for 14.9 and 14.6% of the total protein, respectively. Of note, a mass value of 86.3 kDa was estimated for the 5.7 S species, fitting the mass of a hexamer. Thus, the sedimentation-velocity data are in favour of the formation of discrete oligomers by self-association of dimers at the protein concentration used for crystallization. Under similar conditions [5%(*v*/*v*) 2-propanol in 2 *M* ammonium sulfate solution pH 5.6] CG-1A is a dimer (Varela *et al.*, 1999), as is also the case for CG-1B (López-Lucendo *et al.*, 2009) and hGal-2 (Lobsanov *et al.*, 1993). However, several cases are known with evidence of oligomerization: lectin 2 from the basidomycete *Coprinus cinereus* (inky cap mushroom; Cooper *et al.*, 1997; López-Lucendo, Giménez-Gallego *et al.*, 2004; Walser *et al.*, 2004), the N-domain of mouse galectin-4 (Krejčiříková *et al.*, 2011) and the galectin from the marine sponge *Cinachyrella* sp. (Freymann *et al.*, 2012), all of which crystallize as tetramers. Furthermore, hGal-1, which is present as a dimer in the crystals (López-Lucendo, Solis *et al.*, 2004), forms a dimer of dimers of cylindrical shape in solution in dimethyl sulfoxide (He *et al.*, 2003). It is thus noteworthy that given appropriate conditions the mentioned galectins can self-associate into a quaternary structure beyond dimers. However, the formation of a trimer of dimers is still a unique feature of CG-2.

3.2. Monomer architecture

Looking at the CG-2 monomer, it adopts the typical galectin fold in which two antiparallel β-sheets of six (S1–S6) and five (F1–F5) β-strands, connected by several loops, form a β-sandwich structure (Fig. 2*b*). Topological alignment of the monomers revealed no significant conformational differences; the r.m.s. deviations at the level of C^{α}-atom positions were low (0.30 Å for 130 atoms). Only two of the six binding sites in the crystallographic asymmetric unit host a ligand (Fig. 2*b*). Crystal packing leads to blocking of the other four binding sites, in which a lactose molecule cannot be accommodated because of steric clashes (Supplementary Fig. S1[1]).

With these data in hand, it was possible to address the issue of whether CG-2 will present structural traits that are more akin to hGal-2 (interspecies comparison) than to CG-1A and CG-1B (intraspecies comparison) and hGal-1. Examining the superposed structures of these five galectins (Fig. 2*c*), there indeed is a difference in the S4–S5 loop which connects the antiparallel β-strands S4 and S5. This loop is four residues shorter in CG-2 and hGal-2 compared with hGal-1, CG-1A and CG-1B, in which the four additional amino acids protrude into the solvent (Ala-His-Gly-Asp in hGal-1, Cys-His-Gly-Asp in CG-1A and Ala-His-Gly-Asp in CG-1B). This special feature furnishes CG-2 and hGal-2 with an open cavity in this region, unlike the relatively narrow space in the vicinity of the carbohydrate-binding site of the galectin-1 proteins, with potential consequences for ligand binding (see below). The inspection of the structures also revealed a minor local conformational change in the F5 β-strand of CG-2 and hGal-2 compared with hGal-1, CG-1A and CG-1B (Fig. 2*c*), despite the high conservation of residues in this region (Fig. 1*a*).

3.3. Dimer interface

The canonical dimer interface is formed by the S1 and F1 β-strands from the N- and C-termini of each subunit (Fig. 3*a*). They face each other to set up a large antiparallel β-sheet. The sequence deviations shown in Fig. 1 allow changes in the architecture to become likely. Indeed, the hydrogen-bonding pattern between the S1 β-strands harbours a distinct number of interactions, with four pairs of backbone hydrogen bonds

[1] Supplementary material has been deposited in the IUCr electronic archive (Reference: WD5210). Services for accessing this material are described at the back of the journal.

between Met4, Glu6 and Phe8, whereas only two residues are involved in the other listed proteins (Glu6 and Lys8 in hGal-2, Val6 and Ser8 in hGal-1, and Val6 and Thr8 in CG-1A and CG-1B). On the other side of the interface, the two antiparallel F1 strands establish four pairs of backbone hydrogen bonds involving Thr126, Phe128 and Val130, as similarly observed in hGal-1, hGal-2, CG-1A and CG-1B.

Apart from this polar network, hydrophobic interactions also contribute significantly to the stability of the dimer. The distribution of nonpolar side chains from both the S1 (Met4, Phe5 and Met7) and F1 (Val125, Phe128 and Val130) strands shapes a hydrophobic surface that partakes in dimer assembly. The most striking characteristic of the CG-2 dimer interface is the way that the side chains of Phe5 and Phe128 become key constituents of the hydrophobic pocket (Fig. 3*b*). hGal-2 shares only one of these two Phe residues in the sequence (Fig. 1*a*). Furthermore, CG-2 extends the hydrophobic core by recruiting additional methionine side chains in positions 4 and 7. These two methionines are characteristic of CG-2, revealing that the sequence diversification of galectin-2 proteins after the ancestral gene duplication in these two organisms has resulted in more than conservative differences.

In addition, the relative orientation of the monomers sets the CG-2 dimer apart from the canonical dimer displayed by the prototype galectin-1 family (hGal-1, CG-1A and CG-1B) and also by hGal-2. Using superposition, the relatively large change in the arrangement of subunits in the CG-2 dimer is clearly seen in Fig. 4, with hGal-1 as a control. A large rotation (∼25°) must be applied to bring the second subunit of the CG-2 dimer into its position in hGal-1. As a result, the extended β-sheet is less distorted in CG-2 than in CG-1A, CG-1B and the two human galectins. These disparities, given the similar overall fold of the monomers, are unlikely to be caused by crystal-packing forces involving other regions of the protein (Fig. 2*a*). In detail, the three dimers present in the crystal asymmetric unit can readily be placed onto each other with r.m.s. deviations for all C^{α} atoms of 0.8 Å. Obviously, the fine structure of the interface and the shape distinguish CG-2 from CG-1A, CG-1B, hGal-1 and hGal-2. These features can account for the distinct hydrodynamic behaviour of CG-2 reported previously based on gel filtration, ultracentrifugation and measurement of the diffusion constant (Beyer *et al.*, 1980; Kaltner *et al.*, 2008; Göhler *et al.*, 2012).

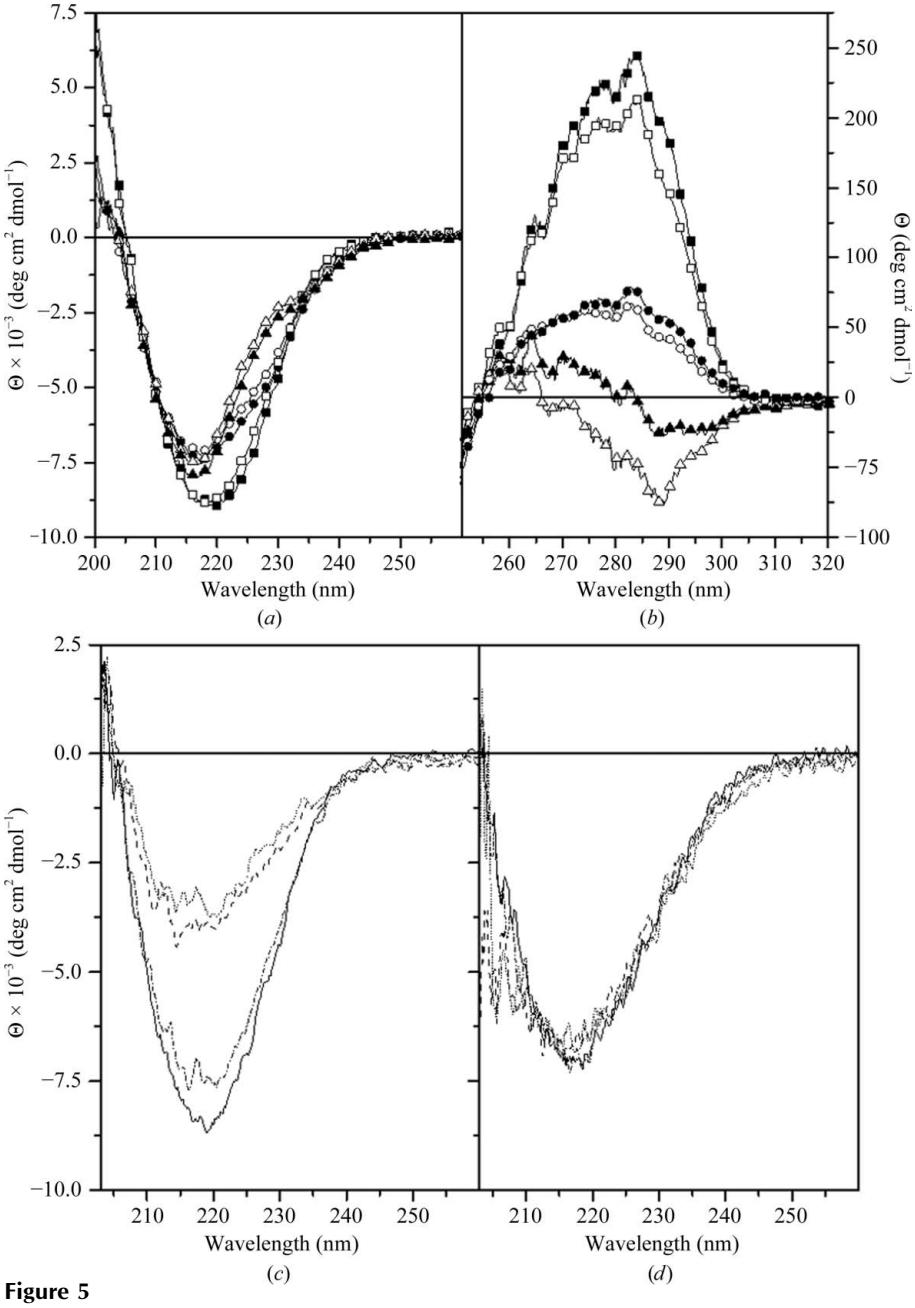

Figure 5
CD spectra of the three prototype CGs. The far-UV (*a*) and near-UV (*b*) CD spectra of CG-2 (squares), CG-1A (circles) and CG-1B (triangles) were obtained at 293 K for 0.2 and 1 mg ml^{-1} solutions, respectively, in PBS$_{\beta}$ in the absence (open symbols) and the presence (solid symbols) of 0.1 *M* lactose. (*c*, *d*) Far-UV spectra of CG-2 (*c*) and CG-1A (*d*) recorded at 303 K (solid line), 323 K (dashed/dotted line), 333 K (CG-2)/343 K (CG-1A) (dashed line) and 363 K (dotted line).

3.4. Structure and stability in solution

In the first step, the far-UV CD spectrum of CG-2 was determined. The presence of a positive signal at 200 nm, together with a negative band centred at 219 nm (Fig. 5*a*), is indicative of a β-sheet structure. Spectra obtained in the absence and the presence of 0.1 *M* lactose indicated that there were no significant changes in secondary

structure upon ligand binding in solution, which is in agreement with the crystallographic results. Comparison with the far-UV CD spectra of CG-1A and CG-1B (Fig. 5*a*) revealed smaller ellipticity signals for the two hGal-1 orthologues and a shift of the minimum towards 217 nm. Of further note, the spectra of CG-1A and CG-1B were significantly different from each other in the 220–234 nm region. These differences are compatible with the presentation of distinctive structural features by each protein such as the length and/or the relative orientation of β-strands, sheets and/or loops.

The near-UV CD spectrum of CG-2 was characterized by the presence of a broad positive signal from 254 to 305 nm with defined bands at 277 and 284 nm in the tyrosine region and a faint shoulder at 290 nm attributable to tryptophan (Fig. 5*b*). The intensity of these signals increased perceptibly in the presence of lactose, pointing to changes in the environment of tyrosine and tryptophan residues upon ligand binding, while the phenylalanine region (254–270 nm) was not affected. Moving on to the comparison of the three CGs, the overall shape of the near-UV CD spectrum of CG-1A was similar, although the signal intensity was reduced. Moreover, the influence of lactose binding was rather small and was restricted to the region 280–295 nm, probably owing to changes in the environment of the tryptophan residue located at the binding site. On the other hand, the spectrum of CG-1B presented a negative band centred at 288 nm and the binding of lactose substantially affected the whole spectrum, including the region attributable to phenylalanine residues.

The fact that the three prototype CGs are sensitive to lactose binding to different degrees was also reflected by their responses to the presence of lactose when measuring the diffusion constant: its value increased by 5.6% for CG-1B, as did that of hGal-1 (He *et al.*, 2003; Göhler *et al.*, 2010), whereas it decreased by 3.8% for CG-2 and remained unchanged for CG-1A (Göhler *et al.*, 2012), in line with the lactose-induced changes observed in the CD spectra.

Stepwise heating of CG-2 resulted in a loss of tertiary and secondary structure, as shown by a progressive decrease of the ellipticity signals both in the near-UV and far-UV CD spectra (Fig. 5*c*). CG-1B underwent similar changes, while for CG-1A changes were only apparent in the near-UV region. In contrast, the far-UV spectrum remained basically unaltered, with only a slight increase in negative ellipticity and significant noise below 210 nm at temperatures of 343 K and above

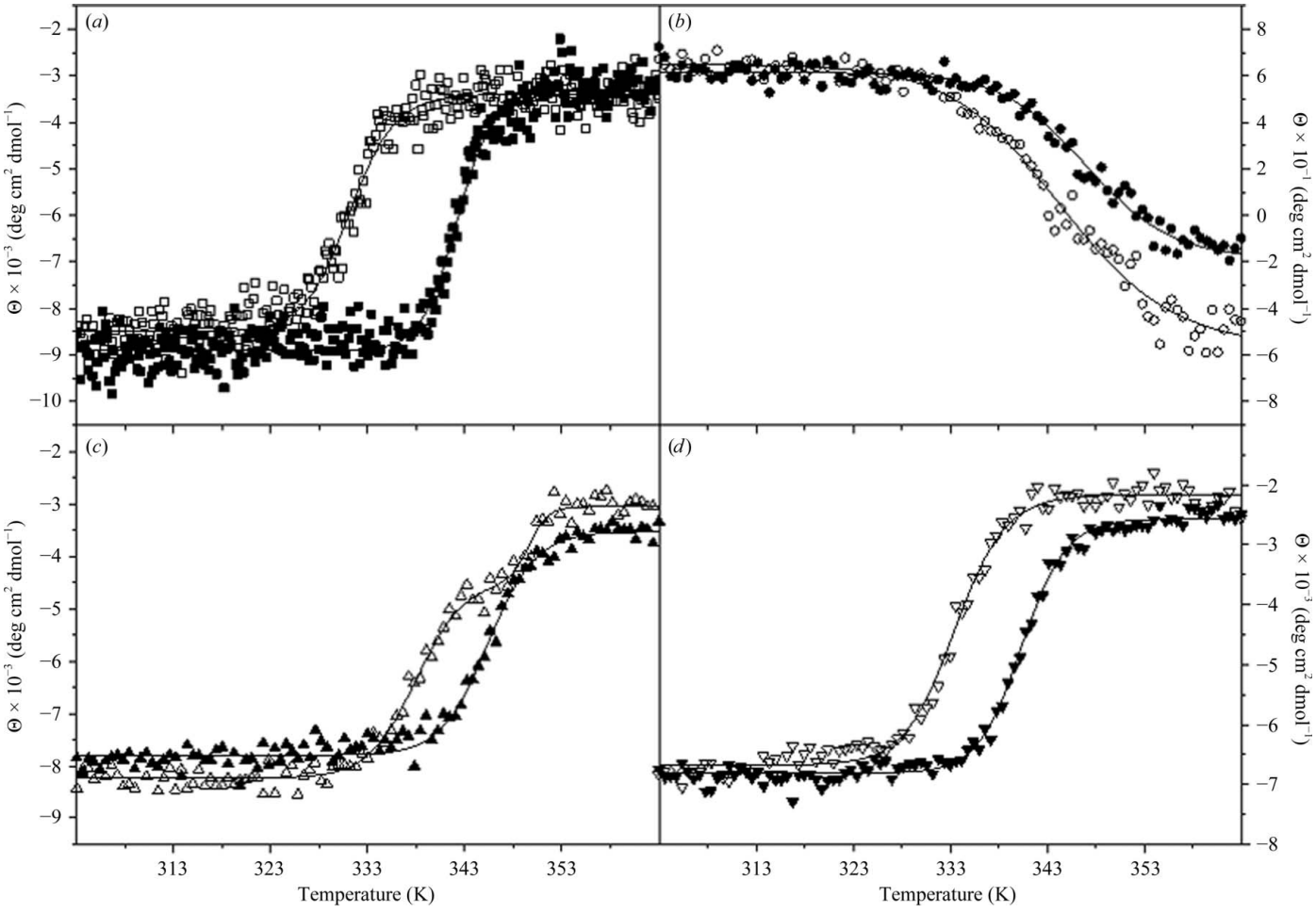

Figure 6
Thermal denaturation profiles of CG-2 (*a*), CG-1A (*b*), CG-1B (*c*) and the C7S mutant of CG-1B (*d*). The variation in ellipticity with temperature was measured either at 217 nm (*a*, *c*, *d*) or at 270 nm (*b*) in the absence (open symbols) and in the presence (solid symbols) of 0.1 *M* lactose for 0.2 mg ml^{-1} (*a*, *c*, *d*) and 1 mg ml^{-1} (*b*) protein solutions in PBS$_\beta$. The continuous lines correspond to the fit of sigmoidal functions to the experimental data.

(Fig. 5*d*). The denaturation process was monitored by measuring the decrease in ellipticity at an appropriate wavelength, *i.e.* 217 nm for CG-2/CG-1B and 270 nm for CG-1A, as a function of temperature (Fig. 6). Denaturation was irreversible and the experimental curves were analyzed phenomenologically using a sigmoidal function (see §2.4), yielding the $T_{1/2}$ values that are compiled in Table 2. Both CG-2 and CG-1A denatured in a single cooperative process (Figs. 6*a* and 6*b*), similar to that observed for hGal-1 (Nesmelova *et al.*, 2010).

Table 2
Transition temperatures of thermal denaturation of prototype chicken galectins monitored by circular dichroism.

	$T_{1/2}$ (K)	
Galectin	No lactose	With 0.1 *M* lactose
CG-2	331.0 ± 0.15	342.6 ± 0.1
CG-1A	344.6 ± 0.25	347.1 ± 0.2
CG-1B		
Wild type	338.1 ± 0.2 349.7 ± 0.2	345.5 ± 0.1
C7S mutant	333.6 ± 0.1	340.5 ± 0.1

Intriguingly, the denaturation profile of CG-1B showed two transitions (Fig. 6*c*) with a difference in $T_{1/2}$ of 11.6 K. Owing to previous experiments, which revealed the formation of intramolecular (Cys2–Cys7) and intermolecular (Cys7–Cys7) disulfide bonds in CG-1B associated with protein oxidation (López-Lucendo *et al.*, 2009), the presence of these linkages in the thermally denatured protein was checked. Gel electrophoresis revealed the presence of a minor population of covalently linked dimers, while mass-spectrometric fingerprint analyses showed the formation of the intramolecular Cys2–Cys7 disulfide, with the intensity of the respective ion being about 60% of that of the species without disulfide bridging. This result prompted the additional analysis of the C7S mutant of CG-1B. Its denaturation profile had a single transition (Fig. 6*d*), indicating that the two transitions observed for the wild-type protein were linked to the formation of disulfide-bonded species. Equally important in quantitative terms, the $T_{1/2}$ obtained for the mutant was within the range found for CG-2 and clearly below that for CG-1A. Thus, despite the detected disparities in the interface, the thermal stabilities of CG-2 and CG-1B appear to be similar.

The impact of ligand binding on the thermal stability of the three CGs was also assessed. In all three cases, the $T_{1/2}$ increased with lactose binding, with the only exception being the second transition observed in the denaturation profile of CG-1B (Table 2). However, the increase in stability differed markedly between the CGs, with CG-2 being the frontrunner with a $T_{1/2}$ difference of 11.6 K. The corresponding value for CG-1A was 2.5 K (Table 2). The apparently protein-specific effect of lactose binding could derive from distinct ligand-induced structural changes, but it may also reflect non-identical modes of binding and affinities. Thus, we next present details on the architecture of the binding site.

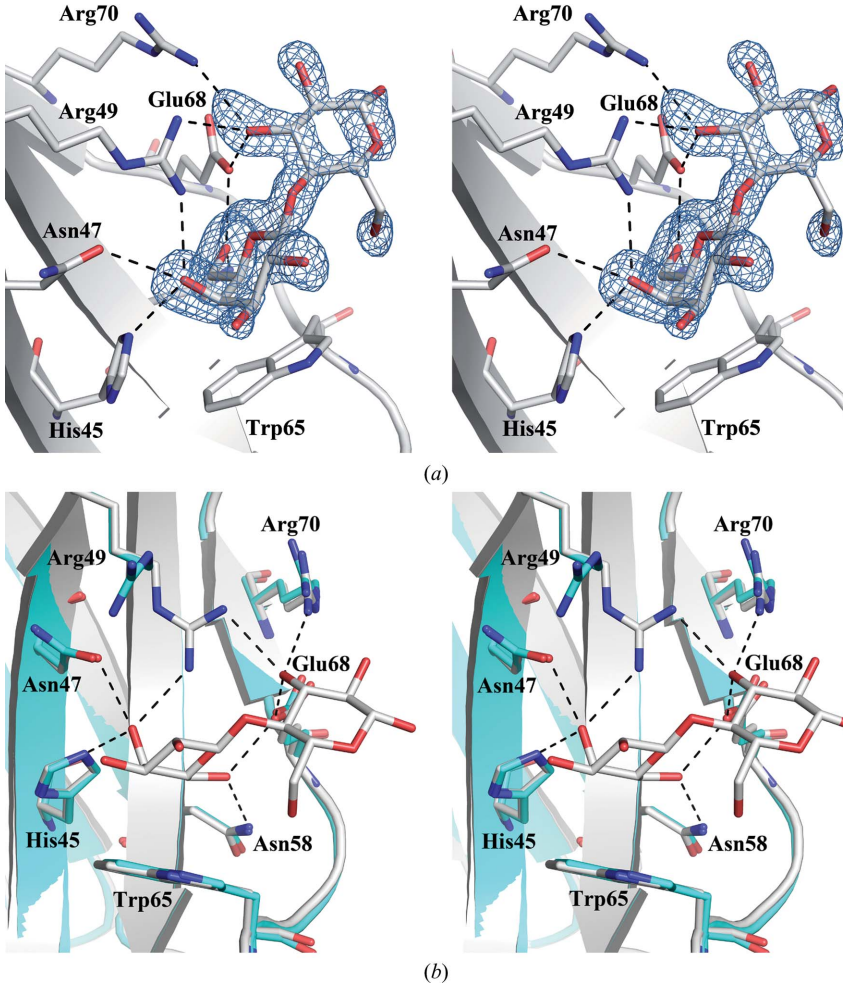

Figure 7
Carbohydrate-binding site of CG-2. (*a*) The lactose moiety and the amino acids of the hydrogen-bond network with the sugar are shown in stick mode. Observed electron-density map of lactose in an $F_o - F_c$ OMIT map contoured at 2.0σ. (*b*) Superposition of this site of CG-2 in ligand-loaded (grey) and ligand-free (cyan) forms.

3.5. Carbohydrate-binding site

The concave surface of the β-sheet, comprising residues from β-strands S4–S6, constitutes the contact site for β-galactosides (Fig. 7*a*). Reflecting the common sequence signature of CGs (Kaltner *et al.*, 2008), a series of conserved amino-acid residues is present in this region, *i.e.* His45, Asn47, Arg49, Asn58, Trp65, Glu68 and Arg70. As noted above, two of the six CG-2 monomers in the crystallographic asymmetric unit were occupied by lactose. The bound conformer corresponds to the low-energy (*syn*) state, extending the data basis for conformer selection by CG-1A and hGal-1 in solution (Siebert *et al.*, 1996, 2003; Asensio *et al.*, 1999; Alonso-Plaza *et al.*,

Table 3
Thermodynamic parameters for lactose binding to the prototype chicken galectins as determined by ITC.

Protein	Buffer	K_a (M^{-1})	ΔG (kcal mol^{-1})	ΔH (kcal mol^{-1})	ΔS (cal mol^{-1} K^{-1})
CG-2	PBS_β	6000 ± 300	−5.14 ± 0.03	−11.1 ± 0.9	−20 ± 3
CG-1A	PBS_β	9000 ± 700	−5.38 ± 0.06	−12.1 ± 0.7	−23 ± 2
CG-1B					
Wild type	PBS_β	1790 ± 200	−4.42 ± 0.07	−4.1 ± 0.3	1 ± 0.7
	$HEPES_\beta$	2230 ± 20	−4.55 ± 0.01	−4.46 ± 0.02	0.4 ± 0.09
C7S mutant	PBS_β	1600 ± 200	−4.36 ± 0.07	−9.0 ± 0.4	−16 ± 1

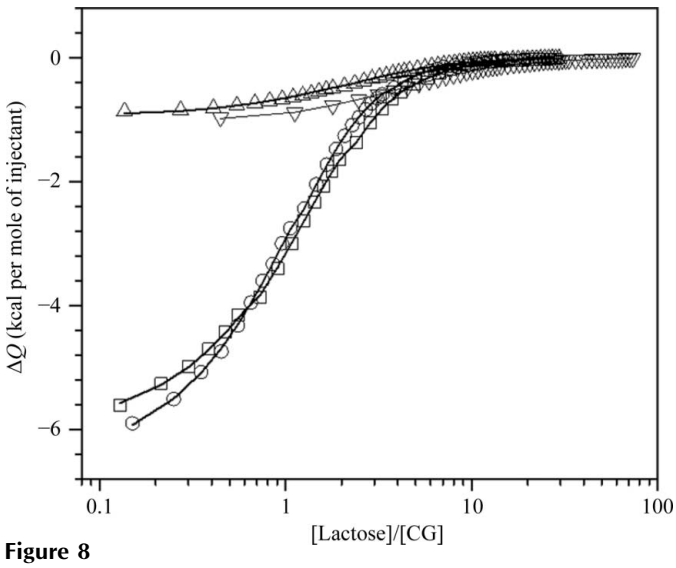

Figure 8
Representative calorimetric titrations of CG-2, CG-1A, CG-1B and the C7S mutant of CG-1B with lactose. Symbols represent the heat released per mole of lactose injected as a function of the molar ratio of lactose and CG; the solid lines correspond to the best fit of the experimental data based on a one-set-of-sites model. Titrations were carried out at 298 K by two successive series of injections of 11–13 m*M* lactose aliquots into the sample cell containing solutions with monomer concentrations of 192 µ*M* CG-2 (squares), 150 µ*M* CG-1A (circles), 196 µ*M* CG-1B (triangles) or 80 µ*M* of the C7S mutant of CG-1B (inverted triangles) in PBS_β.

2001; García-Aparicio *et al.*, 2007; Solís *et al.*, 2009). When bound, the hydroxyl groups at the 4′ and 6′ positions of galactose are the key contact sites for hydrogen bonding: the axial 4′-OH of galactose establishes such interactions with the functional groups of the well conserved residues His45, Asn47 and Arg49, while the hydroxyl group at the 6′ position is hydrogen-bonded to Asn58 and Glu68. The glucose ring engages in hydrogen bonds to Arg49, Glu68 and Arg70 through its 3-OH group, with the latter two residues also being connected by a hydrogen bond. The invariant impact of the presence of lactose on the Trp signals in CD spectroscopy is structurally explained by the C–H/π-interaction with Trp65, as also observed in hGal-1 and hGal-2 (López-Lucendo, Solís *et al.*, 2004; Lobsanov *et al.*, 1993).

Comparison of the architecture of the binding sites reveals that both CG-2 and hGal-2 share contact of the glucose ring with Arg70 *via* a hydrogen bond. This addition to the common hydrogen-bond network in the recognition of lactose by galectins is favoured by the presence of the conserved acidic residue Glu68. It is appropriately located for a salt-bridge interaction with Arg70, thereby positioning its guanidinium group close to the equatorial 3-OH of glucose (Arg70 NE–O3 distances of 3.1 and 2.8 Å in CG-2 and h-Gal2, respectively; Fig. 7*b*). In hGal-1, as well as in CG-1A and CG-1B, the corresponding Arg residue is too far from the 3-OH to make contact with this group. Owing to the presence of the short S4–S5 loop in CG-2 and hGal-2, the open space in the region above position 3 of glucose enables the accommodation of an axial hydroxyl group, although with a concomitant decrease in binding affinity owing to the loss of contacts of the equatorial 3-OH, as observed for the binding of the 3-epi-derivative of methyl β-lactoside to CG-2 (Solís *et al.*, 1996). In contrast, in hGal-1, as also in CG-1A and CG-1B, the longer S4–S5 loop places the conserved His52 at a distance of 4.8 Å from C3 of glucose. Whereas this placement of His52 maintains contacts with the galactose moiety, it may hinder the accommodation of axial substituents at position 3 of glucose.

3.6. Thermodynamic parameters of lactose binding

The thermodynamic parameters for the binding of lactose to CG-2 were assessed using isothermal titration calorimetry (ITC). The heat produced per mole of ligand injected as a function of the [lactose]/[CG] ratio is shown in Fig. 8. Experimental data obtained at 298 K in PBS_β could be fitted using a one-set-of-sites model compatible with the presence of 1.08 ± 0.01 binding sites per CG-2 subunit with an association constant of 6000 ± 300 M^{-1} and with ΔH and ΔS values of −11.1 ± 0.9 kcal mol^{-1} and −20 ± 3 cal mol^{-1} K^{-1}, respectively (Table 3; 1 cal = 4.186 J). Comparable parameters were obtained for CG-1A under similar conditions, with this galectin exhibiting a perceptibly higher affinity derived from a larger enthalpic contribution to the binding. In contrast, the enthalpy change observed for CG-1B was noticeably smaller. It resulted in an association constant that was threefold to fivefold lower than those obtained for the other two prototype CGs, despite the rather atypically lower ΔS value (of close to zero).

In order to investigate the origin of these unusual parameters, other possible events that could contribute to the overall energetics of the process were explored. Titration of CG-1B with lactose in $HEPES_\beta$ yielded very similar thermodynamic parameters (Table 3), thus excluding a sizeable contribution of buffer ionization owing to variations in the pK_a values of protein induced by ligand binding (see §2.5). To evaluate the potential impact of disulfide-bridge formation in CG-1B during titration, the thermodynamic parameters of lactose binding to the C7S mutant were measured. As shown in Table 3, ΔH and ΔS values calculated from the analysis approached those obtained for CG-2 and CG-1A, although the binding affinity remained in the same range, as the gain in favourable enthalpy was counteracted by a loss of entropy. The observed variations in the enthalpy and entropy of

binding between CG-1B and its C7S mutant indicated that disulfide bridging is a major factor to be reckoned with.

Overall, the results indicate that there is not a clear-cut correlation between the different architectures of the carbohydrate-binding sites of CG-2 *versus* CG-1A and CG-1B and the thermodynamic parameters of lactose binding. CG-1A and CG-1B already differ in the contributions to the Gibbs free energy. Interestingly, CG-1B, the protein which undergoes the largest ligand-induced changes in the near-UV CD spectrum, has the lowest binding affinity, whereas CG-1A, which displays rather small alterations in the spectrum, shows the highest affinity. These observations hint at the likely bearing of conformational rearrangements at sites other than the contact region for the ligand on the overall energetics of the binding process, which may vary with the nature of the ligand. Interestingly, the conformational entropy of the CRD of hGal-3 has been reported to be increased upon lactose binding without a major structural change, leading to the suggestion that affecting this parameter could conversely impact on the affinity of ligand binding (Diehl *et al.*, 2009). As this example attests, altering the conformational entropy will not necessarily engender an effect on the shape, because the diffusion constant of hGal-3 is not affected by ligand loading (Göhler *et al.*, 2010).

4. Conclusions

The presented information on CG-2 completes the crystallographic analysis of homodimeric galectins in the chicken model system. A shortened loop between strands S4 and S5, regional differences in the area of ligand contact and unique features in the interface were detected. Since counter-receptor selection critically depends on carbohydrate specificity and topological features (Murphy *et al.*, 2013), the potential of CG-2 dimers to self-associate at high local concentration could explain its significantly higher abundance at saturation on the surface of avian B cells compared with CG-1A, despite a rather similar pattern of reactive glycoproteins for the two lectins (Schneller *et al.*, 1995). This potential, which can be favoured by topologically suited counter-receptor presentation in microdomains (Stechly *et al.*, 2009; Kopitz *et al.*, 2010; Velasco *et al.*, 2013), may be physiologically relevant. This is the case for induction of pentamerization of the chimera-type Gal-3 by polyvalent ligands in model systems with synthetic ligands and *in vitro* (Ahmad *et al.*, 2004; Kopitz *et al.*, 2010). Here, the monomeric lectin turns into a competitive inhibitor of binding of homodimeric (cross-linking) proteins. The case of the tumour suppressor $p16^{INK4a}$, which recruits hGal-1 to drive tumour cells into anoikis and at the same time down-regulates Gal-3 availability, provides an example of functional divergence in a physiological context (André *et al.*, 2007; Sanchez-Ruderisch *et al.*, 2010).

Together with the tight regulation of expression of the three prototype CGs with few cases of overlaps in the respective profiles (Kaltner *et al.*, 2008; Kaltner & Gabius, 2012), these structural insights intimate a low degree of functional redundancy. An excellent example of this concept is the preferential expression of CG-1A in the zeugopod region of five-day leg buds and its role in cell self-organizing dynamics to generate condensations and to let cartilage mature in chicken limb skeletal morphogenesis (Bhat *et al.*, 2011). The interplay with the tandem-repeat-type CG-8 in this process cascade certainly provides an incentive to characterize this family member to the same extent. Of medical interest, a genetic polymorphism in the coding region of the N-terminal CRD of human galectin-8 (the F19Y variant) has been associated with autoimmune diseases (Pál *et al.*, 2012). Recalling the peculiar hydrodynamic behaviour of CG-2, explaining how the individual pattern of structural dynamics and flexibility is encoded in the sequence of the CGs is an attractive challenge, as is to complete the crystallographic analysis for all five CGs along with their spectroscopic and thermodynamic characterization.

This work has been kindly supported by grants BFU2009-10052, BFU2011-24615, BFU2012-36825 and CSD2009-00088 from the Spanish Ministry of Science and Innovation, the CIBER of Respiratory Diseases (CIBERES), an initiative from ISCIII, the Regional Government of Madrid (S2010/BMD-2353) and by funding from the European Union's Seventh Framework Program FP7/2007–2013 under REA grant agreements Nos. 260600 ('GlycoHIT') and 317297 ('GLYCOPHARM'). FMR and LL-M were supported by JAE-DOC and JAE_PRE grants, respectively, from CSIC, Spain. Finally, the authors cordially thank the staff of beamline ID14-2 at the ESRF, Grenoble for generous support.

References

Ahmad, N., Gabius, H.-J., André, S., Kaltner, H., Sabesan, S., Roy, R., Liu, B., Macaluso, F. & Brewer, C. F. (2004). *J. Biol. Chem.* **279**, 10841–10847.

Alonso-Plaza, J. M., Canales, M. A., Jiménez, M., Roldán, J. L., García-Herrero, A., Iturrino, L., Asensio, J. L., Cañada, F. J., Romero, A., Siebert, H.-C., André, S., Solís, D., Gabius, H.-J. & Jiménez-Barbero, J. (2001). *Biochim. Biophys. Acta*, **1568**, 225–236.

Amano, M., Eriksson, H., Manning, J. C., Detjen, K. M., André, S., Nishimura, S., Lehtiö, J. & Gabius, H.-J. (2012). *FEBS J.* **279**, 4062–4080.

André, S., Jarikote, D. V., Yan, D., Vincenz, L., Wang, G.-N., Kaltner, H., Murphy, P. V. & Gabius, H.-J. (2012). *Bioorg. Med. Chem. Lett.* **22**, 313–318.

André, S., Kaltner, H., Lensch, M., Russwurm, R., Siebert, H.-C., Fallsehr, C., Tajkhorshid, E., Heck, A. J. R., von Knebel Doeberitz, M., Gabius, H.-J. & Kopitz, J. (2005). *Int. J. Cancer*, **114**, 46–57.

André, S. *et al.* (2007). *FEBS J.* **274**, 3233–3256.

Asensio, J. L., Espinosa, J. F., Dietrich, H., Cañada, F. J., Schmidt, R. R., Martín-Lomas, M., André, S., Gabius, H.-J. & Jiménez-Barbero, J. (1999). *J. Am. Chem. Soc.* **121**, 8995–9000.

Barondes, S. H., Cooper, D. N., Gitt, M. A. & Leffler, H. (1994). *J. Biol. Chem.* **269**, 20807–20810.

Beyer, E. C. & Barondes, S. H. (1982). *J. Cell Biol.* **92**, 23–27.

Beyer, E. C., Zweig, S. E. & Barondes, S. H. (1980). *J. Biol. Chem.* **255**, 4236–4239.

Bhat, R., Lerea, K. M., Peng, H., Kaltner, H., Gabius, H.-J. & Newman, S. A. (2011). *BMC Dev. Biol.* **11**, 6.

Campanero-Rhodes, M. A., Menéndez, M., Saiz, J. L., Sanz, L., Calvete, J. J. & Solís, D. (2006). *Biochemistry*, **45**, 8227–8235.

Chen, V. B., Arendall, W. B., Headd, J. J., Keedy, D. A., Immormino, R. M., Kapral, G. J., Murray, L. W., Richardson, J. S. & Richardson, D. C. (2010). *Acta Cryst.* D**66**, 12–21.

Cooper, D. N. W. (2002). *Biochim. Biophys. Acta*, **1572**, 209–231.
Cooper, D. N. W., Boulianne, R. P., Charlton, S., Farrell, E. M., Sucher, A. & Lu, B. C. (1997). *J. Biol. Chem.* **272**, 1514–1521.
DeLano, W. L. (2002). *PyMOL*. http://www.pymol.org.
Diehl, C., Genheden, S., Modig, K., Ryde, U. & Akke, M. (2009). *J. Biomol. NMR*, **45**, 157–169.
Emsley, P., Lohkamp, B., Scott, W. G. & Cowtan, K. (2010). *Acta Cryst.* D**66**, 486–501.
Freymann, D. M., Nakamura, Y., Focia, P. J., Sakai, R. & Swanson, G. T. (2012). *Acta Cryst.* D**68**, 1163–1174.
Gabius, H.-J. (1997). *Eur. J. Biochem.* **243**, 543–576.
Gabius, H.-J. (2009). Editor. *The Sugar Code. Fundamentals of Glycosciences.* Weinheim: Wiley-VCH.
Gabius, H.-J., André, S., Jiménez-Barbero, J., Romero, A. & Solís, D. (2011). *Trends Biochem. Sci.* **36**, 298–313.
Gabius, H.-J., Engelhardt, R., Rehm, S. & Cramer, F. (1984). *J. Natl Cancer Inst.* **73**, 1349–1357.
García-Aparicio, V., Sollogoub, M., Blériot, Y., Colliou, V., André, S., Asensio, J. L., Cañada, F. J., Gabius, H.-J., Sinaÿ, P. & Jiménez-Barbero, J. (2007). *Carbohydr. Res.* **342**, 1918–1928.
Göhler, A., André, S., Kaltner, H., Sauer, M., Gabius, H.-J. & Doose, S. (2010). *Biophys. J.* **98**, 3044–3053.
Göhler, A., Büchner, C., André, S., Doose, S., Kaltner, H. & Gabius, H.-J. (2012). *Biochimie*, **94**, 2649–2655.
He, L., André, S., Siebert, H.-C., Helmholz, H., Niemeyer, B. & Gabius, H.-J. (2003). *Biophys. J.* **85**, 511–524.
Hirabayashi, J., Kawasaki, H., Suzuki, K. & Kasai, K. (1987). *J. Biochem.* **101**, 775–787.
Houzelstein, D., Gonçalves, I. R., Fadden, A. J., Sidhu, S. S., Cooper, D. N., Drickamer, K., Leffler, H. & Poirier, F. (2004). *Mol. Biol. Evol.* **21**, 1177–1187.
Kaltner, H. & Gabius, H.-J. (2012). *Histol. Histopathol.* **27**, 397–416.
Kaltner, H., Solís, D., Kopitz, J., Lensch, M., Lohr, M., Manning, J. C., Mürnseer, M., Schnölzer, M., André, S., Sáiz, J. L. & Gabius, H.-J. (2008). *Biochem. J.* **409**, 591–599.
Karplus, P. A. & Diederichs, K. (2012). *Science*, **336**, 1030–1033.
Kasai, K. & Hirabayashi, J. (1996). *J. Biochem.* **119**, 1–8.
Klyosov, A. A., Witczak, Z. J. & Platt, D. (2008). *Galectins.* Hoboken: John Wiley & Sons.
Kopitz, J., Bergmann, M. & Gabius, H.-J. (2010). *IUBMB Life*, **62**, 624–628.
Krejčiříková, V., Pachl, P., Fábry, M., Malý, P., Řezáčová, P. & Brynda, J. (2011). *Acta Cryst.* D**67**, 204–211.
Krissinel, E. & Henrick, K. (2007). *J. Mol. Biol.* **372**, 774–797.
Leslie, A. G. W. (2006). *Acta Cryst.* D**62**, 48–57.
Lobsanov, Y. D., Gitt, M. A., Leffler, H., Barondes, S. H. & Rini, J. M. (1993). *J. Biol. Chem.* **268**, 27034–27038.
Lohr, M., Lensch, M., André, S., Kaltner, H., Siebert, H.-C., Smetana, K. Jr, Sinowatz, F. & Gabius, H.-J. (2007). *Folia Biol. (Praha)*, **53**, 109–128.
López-Lucendo, M. F., Giménez-Gallego, G., Cooper, D. N. W., Gabius, H.-J. & Romero, A. (2004). *Acta Cryst.* D**60**, 721–724.
López-Lucendo, M. F., Solís, D., André, S., Hirabayashi, J., Kasai, K., Kaltner, H., Gabius, H.-J. & Romero, A. (2004). *J. Mol. Biol.* **343**, 957–970.
López-Lucendo, M. F., Solís, D., Sáiz, J. L., Kaltner, H., Russwurm, R., André, S., Gabius, H.-J. & Romero, A. (2009). *J. Mol. Biol.* **386**, 366–378.
Martín-Santamaría, S., André, S., Buzamet, E., Caraballo, R., Fernández-Cureses, G., Morando, M., Ribeiro, J. P., Ramírez-Gualito, K., de Pascual-Teresa, B., Cañada, F. J., Menéndez, M., Ramström, O., Jiménez-Barbero, J., Solís, D. & Gabius, H.-J. (2011). *Org. Biomol. Chem.* **9**, 5445–5455.
Matthews, B. W. (1968). *J. Mol. Biol.* **33**, 491–497.
McCoy, A. J., Grosse-Kunstleve, R. W., Adams, P. D., Winn, M. D., Storoni, L. C. & Read, R. J. (2007). *J. Appl. Cryst.* **40**, 658–674.
Murphy, P. V., André, S. & Gabius, H.-J. (2013). *Molecules*, **18**, 4026–4053.
Murshudov, G. N., Skubák, P., Lebedev, A. A., Pannu, N. S., Steiner, R. A., Nicholls, R. A., Winn, M. D., Long, F. & Vagin, A. A. (2011). *Acta Cryst.* D**67**, 355–367.
Nesmelova, I. V., Ermakova, E., Daragan, V. A., Pang, M., Menéndez, M., Lagartera, L., Solís, D., Baum, L. G. & Mayo, K. H. (2010). *J. Mol. Biol.* **397**, 1209–1230.
Nio-Kobayashi, J., Takahashi-Iwanaga, H. & Iwanaga, T. (2009). *J. Histochem. Cytochem.* **57**, 41–50.
Oka, T., Murakami, S., Arata, Y., Hirabayashi, J., Kasai, K., Wada, Y. & Futai, M. (1999). *Arch. Biochem. Biophys.* **361**, 195–201.
Pál, Z. *et al.* (2012). *Biochim. Biophys. Acta*, **1820**, 1512–1518.
Saal, I., Nagy, N., Lensch, M., Lohr, M., Manning, J. C., Decaestecker, C., André, S., Kiss, R., Salmon, I. & Gabius, H.-J. (2005). *Histol. Histopathol.* **20**, 1191–1208.
Sakakura, Y., Hirabayashi, J., Oda, Y., Ohyama, Y. & Kasai, K. (1990). *J. Biol. Chem.* **265**, 21573–21579.
Sanchez-Ruderisch, H., Fischer, C., Detjen, K. M., Welzel, M., Wimmel, A., Manning, J. C., André, S. & Gabius, H.-J. (2010). *FEBS J.* **277**, 3552–3563.
Schneller, M., André, S., Cihak, J., Kaltner, H., Merkle, H., Rademaker, G. J., Haverkamp, J., Thomas-Oates, J. E., Lösch, U. & Gabius, H.-J. (1995). *Cell. Immunol.* **166**, 35–43.
Schwartz-Albiez, R. (2009). *The Sugar Code. Fundamentals of Glycosciences*, edited by H.-J. Gabius, pp. 447–467. Weinheim: Wiley-VCH.
Siebert, H.-C., André, S., Lu, S.-Y., Frank, M., Kaltner, H., van Kuik, J. A., Korchagina, E. Y., Bovin, N., Tajkhorshid, E., Kaptein, R., Vliegenthart, J. F. G., von der Lieth, C.-W., Jiménez-Barbero, J., Kopitz, J. & Gabius, H.-J. (2003). *Biochemistry*, **42**, 14762–14773.
Siebert, H.-C., Gilleron, M., Kaltner, H., von der Lieth, C.-W., Kozár, T., Bovin, N., Korchagina, E. Y., Vliegenthart, J. F. & Gabius, H.-J. (1996). *Biochem. Biophys. Res. Commun.* **219**, 205–212.
Smetana, K. Jr, André, S., Kaltner, H., Kopitz, J. & Gabius, H.-J. (2013). *Expert Opin. Ther. Targets*, **17**, 379–392.
Solís, D. *et al.* (2010). *Int. J. Biochem. Cell Biol.* **42**, 1019–1029.
Solís, D., Romero, A., Kaltner, H., Gabius, H.-J. & Díaz-Mauriño, T. (1996). *J. Biol. Chem.* **271**, 12744–12748.
Solís, D., Romero, A., Menéndez, M. & Jiménez-Barbero, J. (2009). *The Sugar Code. Fundamentals of Glycosciences*, edited by H.-J. Gabius, pp. 233–245. Weinheim: Wiley-VCH.
Stechly, L., Morelle, W., Dessein, A.-F., André, S., Grard, G., Trinel, D., Dejonghe, M.-J., Leteurtre, E., Drobecq, H., Trugnan, G., Gabius, H.-J. & Huet, G. (2009). *Traffic*, **10**, 438–450.
Stierstorfer, B., Kaltner, H., Neumüller, C., Sinowatz, F. & Gabius, H.-J. (2000). *Histochem. J.* **32**, 325–336.
Stowell, S. R., Arthur, C. M., Mehta, P., Slanina, K. A., Blixt, O., Leffler, H., Smith, D. F. & Cummings, R. D. (2008). *J. Biol. Chem.* **283**, 10109–10123.
Sturm, A., Lensch, M., André, S., Kaltner, H., Wiedenmann, B., Rosewicz, S., Dignass, A. U. & Gabius, H.-J. (2004). *J. Immunol.* **173**, 3825–3837.
Tasumi, S. & Vasta, G. R. (2007). *J. Immunol.* **179**, 3086–3098.
Thomsen, M. K., Hansen, G. H. & Danielsen, E. M. (2009). *Mol. Membr. Biol.* **26**, 347–355.
Vagin, A. & Teplyakov, A. (2010). *Acta Cryst.* D**66**, 22–25.
Varela, P. F., Solís, D., Díaz-Mauriño, T., Kaltner, H., Gabius, H.-J. & Romero, A. (1999). *J. Mol. Biol.* **294**, 537–549.
Velasco, S., Díez-Revuelta, N., Hernández-Iglesias, T., Kaltner, H., André, S., Gabius, H.-J. & Abad-Rodríguez, J. (2013). *J. Neurochem.* **125**, 49–62.
Villalobo, A., Nogales-González, A. & Gabius, H.-J. (2006). *Trends Glycosci. Glycotechnol.* **18**, 1–37.
Walser, P. J., Haebel, P. W., Künzler, M., Sargent, D., Kües, U., Aebi, M. & Ban, N. (2004). *Structure*, **12**, 689–702.
Winn, M. D. *et al.* (2011). *Acta Cryst.* D**67**, 235–242.
Wu, A. M., Singh, T., Liu, J.-H., Krzeminski, M., Russwurm, R., Siebert, H.-C., Bonvin, A. M. J. J., André, S. & Gabius, H.-J. (2007). *Glycobiology*, **17**, 165–184.